LETTER

doi:10.1038/nature13798

Methane dynamics regulated by microbial community response to permafrost thaw

Carmody K. McCalley[1]†, Ben J. Woodcroft[2], Suzanne B. Hodgkins[3], Richard A. Wehr[1], Eun-Hae Kim[4], Rhiannon Mondav[2]†, Patrick M. Crill[5], Jeffrey P. Chanton[3], Virginia I. Rich[4], Gene W. Tyson[2] & Scott R. Saleska[1]

Permafrost contains about 50% of the global soil carbon[1]. It is thought that the thawing of permafrost can lead to a loss of soil carbon in the form of methane and carbon dioxide emissions[2,3]. The magnitude of the resulting positive climate feedback of such greenhouse gas emissions is still unknown[3] and may to a large extent depend on the poorly understood role of microbial community composition in regulating the metabolic processes that drive such ecosystem-scale greenhouse gas fluxes. Here we show that changes in vegetation and increasing methane emissions with permafrost thaw are associated with a switch from hydrogenotrophic to partly acetoclastic methanogenesis, resulting in a large shift in the $\delta^{13}C$ signature (10–15‰) of emitted methane. We used a natural landscape gradient of permafrost thaw in northern Sweden[4,5] as a model to investigate the role of microbial communities in regulating methane cycling, and to test whether a knowledge of community dynamics could improve predictions of carbon emissions under loss of permafrost. Abundance of the methanogen Candidatus '*Methanoflorens stordalenmirensis*'[6] is a key predictor of the shifts in methane isotopes, which in turn predicts the proportions of carbon emitted as methane and as carbon dioxide, an important factor for simulating the climate feedback associated with permafrost thaw in global models[3,7]. By showing that the abundance of key microbial lineages can be used to predict atmospherically relevant patterns in methane isotopes and the proportion of carbon metabolized to methane during permafrost thaw, we establish a basis for scaling changing microbial communities to ecosystem isotope dynamics. Our findings indicate that microbial ecology may be important in ecosystem-scale responses to global change.

Multiple factors—including hydrology, vegetation, organic matter chemistry, pH and soil microclimate—are affected by permafrost loss[5,8,9]. Together these factors regulate microbial metabolisms that release carbon dioxide (CO_2) and methane (CH_4) from thawing permafrost[10–12] and are the basis for Earth-system model predictions of future CH_4 emissions[7,13,14]. However, the role of microbial community composition in regulating the metabolic processes that drive ecosystem-scale fluxes is unknown.

At our study site in Stordalen mire, as in other thawing permafrost peatlands[8,15], permafrost loss causes hydrological and vegetation shifts: well-drained permafrost-supported palsas collapse into partly thawed bogs dominated by moss (*Sphagnum* spp.) and fully thawed fens dominated by sedges (such as *Eriophorum angustifolium*)[4]. Between 1970 and 2000, 10% of Stordalen's palsa habitat thawed into such wetlands[4]. This transition drives an appreciable global warming impact because CO_2-emitting palsa is converted to bogs and fens, which take up CO_2 but emit CH_4 (a more potent greenhouse gas[3])[4,5,16]. The net effect is that the high-methane-emitting fen contributes sevenfold as much greenhouse impact per unit area as the palsa. This thaw progression is also associated with an increase in overall organic matter lability, including a decrease in C:N ratio and an increase in humification rates[9]. We speculated, consistent with previous studies of *in situ* bog and fen systems[17–19], that thaw progression also facilitates a shift from hydrogenotrophic to acetoclastic CH_4 production.

We used the distinct isotopic signatures of different microbial CH_4 production and consumption pathways to directly relate changes in CH_4 dynamics across the thaw gradient to underlying changes in the microbial community. Methane produced by hydrogenotrophic methanogens generally has lower $\delta^{13}C$ and higher δD ($\delta^{13}C = -110‰$ to $-60‰$ and $\delta D = -250‰$ to $-170‰$) relative to that produced by acetoclastic methanogens ($\delta^{13}C = -60‰$ to $-50‰$ and $\delta D = -400‰$ to $-250‰$)[19,20]. If methanotrophic microbes then oxidize CH_4, lighter molecules are preferentially consumed, leaving the remaining CH_4 enriched in ^{13}C and D relative to the original CH_4 pool (expected patterns are shown in Extended Data Fig. 1)[19,20].

High-temporal-resolution measurements of the magnitude and isotopic composition of CH_4 emissions, using a quantum cascade laser spectrometer (Aerodyne Research Inc.) connected to autochambers, showed that CH_4 emissions and their ^{13}C content increased with thaw. Average CH_4 fluxes increased from effectively zero at the intact permafrost palsa site to 1.46 ± 0.37 mg CH_4 m^{-2} h^{-1} (all errors are reported as s.e.m.) at the thawing *Sphagnum* site, and to 8.75 ± 0.50 mg CH_4 m^{-2} h^{-1} at the fully thawed *Eriophorum* site (Fig. 1a; $P < 0.001$). The average $\delta^{13}C$ of emitted CH_4 also increased significantly, from $-79.6 \pm 0.9‰$ in the *Sphagnum* site to $-66.3 \pm 1.6‰$ in the *Eriophorum* site (Fig. 1b; $P = 0.03$). This consistent 10–15‰ divergence between sites was maintained through the growing season but overlain by parallel fluctuations in $\delta^{13}C$-CH_4, suggesting that weather patterns exerted a common influence over the magnitude of isotopic fractionation. Porewater CH_4 isotopes showed a similar pattern, with *Eriophorum* site porewater $\delta^{13}C$ about 10‰ higher than that of *Sphagnum* (July and August; Fig. 1b and Extended Data Table 1). Porewater CH_4 was ^{13}C-enriched by 5–20‰ relative to emitted CH_4, as expected, as a result of diffusive fractionation (Methods, equation (2))[18,21].

The apparent fractionation factor for carbon in porewater CH_4 relative to CO_2, α_C (Methods, equation (2), and Extended Data Table 1), is a related index of changes in CH_4 production[22]. Greater fractionation is associated with hydrogenotrophic methanogenesis and was found in the thawing *Sphagnum* site ($\alpha_C = 1.053 \pm 0.002$). Significantly less fractionation ($P = 0.002$) associated with more acetoclastic production or with consumption by oxidation was found in the fully thawed *Eriophorum* porewater ($\alpha_C = 1.046 \pm 0.001$). Here, increases in acetoclastic production, not oxidation, best explain isotopic shifts because lower α_C and higher $\delta^{13}C$-CH_4 are accompanied by significantly lower δD-CH_4 (Extended Data Fig. 1; $P < 0.001$)[19]. This is consistent with the pattern of isotopes in CH_4 emissions, in incubations of Stordalen peat[9] and in studies showing bog-to-fen shifts from hydrogenotrophic to acetoclastic methanogenesis[17–19].

The CH_4 flux and isotope results provide compelling but indirect evidence for changes in CH_4-cycling microbial communities with permafrost

[1]Department of Ecology and Evolutionary Biology, University of Arizona, Tucson, Arizona 85721, USA. [2]Australian Centre for Ecogenomics, School of Chemistry and Molecular Biosciences, University of Queensland, Brisbane 4072, Queensland, Australia. [3]Department of Earth, Ocean and Atmospheric Science, Florida State University, Tallahassee, Florida 32306, USA. [4]Department of Soil, Water and Environmental Science, University of Arizona, Tucson, Arizona 85721, USA. [5]Department of Geological Sciences, Stockholm University, Stockholm 106 91, Sweden. †Present addresses: Earth Systems Research Center, University of New Hampshire, Durham, New Hampshire 03824, USA (C.K.M.); Department of Ecology and Genetics, Uppsala University, Uppsala 75 236, Sweden (R.M.).

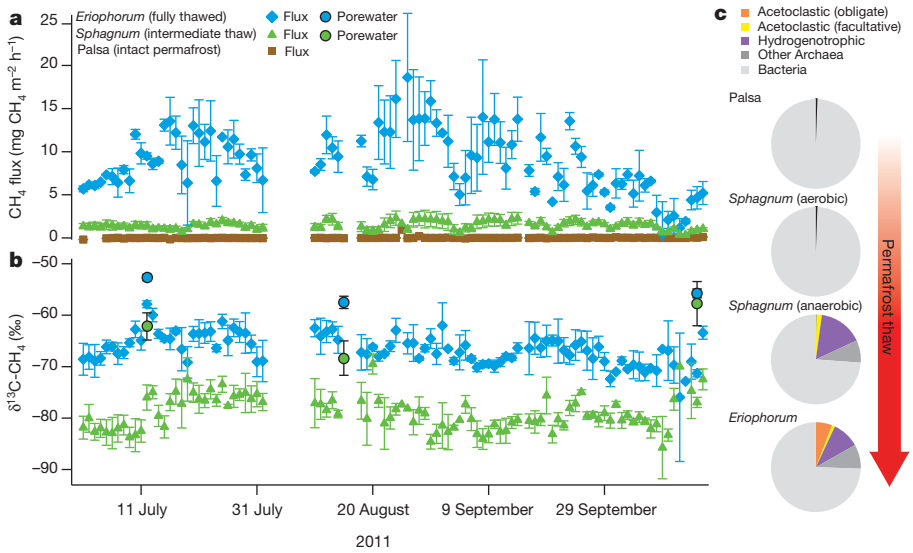

Figure 1 | Increases in the magnitude and $\delta^{13}C$ signature of CH_4 during permafrost thaw track shifts in methanogen communities. **a**, Average daily CH_4 emissions (error bars represent s.e.m.; $n = 2–3$). **b**, $\delta^{13}C$ composition of emitted and porewater CH_4 (error bars represent s.e.m.; flux $n = 2–3$, porewater $n = 6–9$). **c**, Relative abundance of methanogenic groups as inferred by taxonomic identity assigned from 16S rRNA amplicon sequencing ($n = 3$). For the intermediate-thaw *Sphagnum* site, aerobic communities were sampled above the water table; anaerobic communities were sampled below the water table.

thaw. These microbiological changes could be shifts in activity of particular community members or changes in community composition. We examined the role of community composition through 16S rRNA gene amplicon sequencing. All known methanogens belong to a small number of archaeal lineages within the Euryarchaeota[23]. As expected, the shift from CH_4-neutral intact permafrost palsa to CH_4-emitting wetland corresponded to a substantial increase in the relative abundance of methanogenic archaeal lineages (Fig. 1c and Extended Data Table 2, 3). In the aerobic palsa and surface *Sphagnum* habitats, methanogens were found in low relative abundance (average less than 0.6%), whereas the anaerobic environments of the *Eriophorum* and deeper (below the water table) *Sphagnum* habitats harboured communities with a substantially higher relative abundance of methanogens (20–30%).

More significantly, the abundance of specific methanogenic lineages varied across the thaw gradient (Fig. 1c and Extended Data Table 2) in a manner corresponding to shifts in CH_4 production mechanism inferred from the isotope data (Fig. 1b). At the partly thawed *Sphagnum* site, where CH_4 isotopes were more hydrogenotrophic, the methanogen community was dominated by hydrogenotrophic populations (at least 57% of sequences). Members of the genus *Methanobacterium* and close relatives of the recently described hydrogenotroph Candidatus '*Methanoflorens stordalenmirensis*'[6] (a partial genome of which has also been identified in incubations of Alaskan permafrost[12]) were the most abundant phylotypes. Although present, the metabolically versatile *Methanosarcina* (capable of using a wide range of substrates, including acetate and hydrogen[24]), was much less abundant, averaging about 15% of the methanogen sequences. At the fully thawed *Eriophorum* site (where isotope signatures shifted towards acetoclastic), members of the obligately acetoclastic genus *Methanosaeta* increased in abundance, comprising roughly one-third of the methanogenic population. The remaining methanogenic community at the Eriophorum site was taxonomically diverse and included lineages also present at the *Sphagnum* site, as well as the hydrogenotrophic genus, *Methanoregula* (Extended Data Table 2). Differences in the functional (hydrogenotrophic versus acetoclastic) composition of the methanogen community between the sites were smallest in October, coinciding with a convergence in $\delta^{13}C$-CH_4 (Fig. 1a and Extended Data Tables 2 and 3).

Taken together, the isotope and microbial sequence data suggest that shifts in microbial communities drive large, concordant variations in CH_4 isotope biogeochemistry both seasonally and during permafrost thaw, a novel observation at the ecosystem scale. The early successional hydrogenotroph '*M. stordalenmirensis*'[6] dominates methanogenic metabolism in the early stages of thaw, followed by the subsequent emergence of a more diverse methanogen community, including obligate acetoclastic methanogens. This microbial succession provides direct evidence for how changes in ecosystem structure during permafrost thaw (plant succession and increases in organic matter quality[9]) translate into altered CH_4 biogeochemistry.

To quantify the effect of this shifting microbial community composition for CH_4 isotopic patterns, we examined the relationships between isotope fractionation (α_C), environmental conditions known or expected to impact methanogenesis, and the relative abundance of specific methanogenic lineages (Extended Data Table 4). Rather than a functional group (such as hydrogenotrophic methanogens), a single organism—the hydrogenotroph '*M. stordalenmirensis*'—was the best one-variable predictor

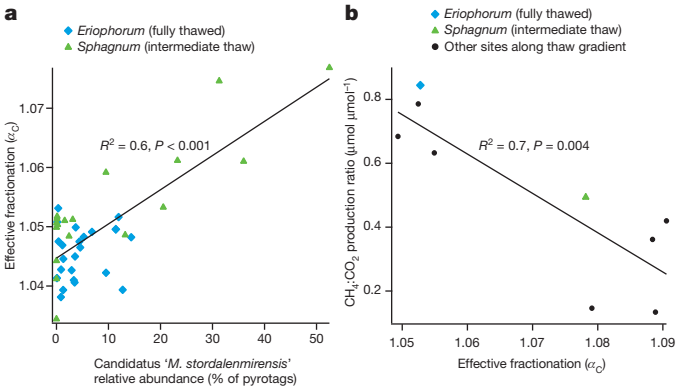

Figure 2 | Correlation between α_C and both Candidatus '*Methanoflorens stordalenmirensis*' and the anaerobic CH_4:CO_2 production ratio. **a**, The relative abundance of a single methanogen, Candidatus '*Methanoflorens stordalenmirensis*', in the field was significantly correlated (linear regression, $P < 0.001$, $n = 41$) with porewater effective fractionation (α_C), an isotopic indicator of the methanogenic production pathway. **b**, Anaerobic incubations of peat collected from a related thaw sequence at Stordalen mire (see methods in ref. 9) show a significant correlation between α_C and the CH_4:CO_2 production ratio (linear regression, $P = 0.004$, $n = 9$), suggesting that the abundance of '*M. stordalenmirensis*' may be indicative of the proportion of organic matter metabolized to CH_4.

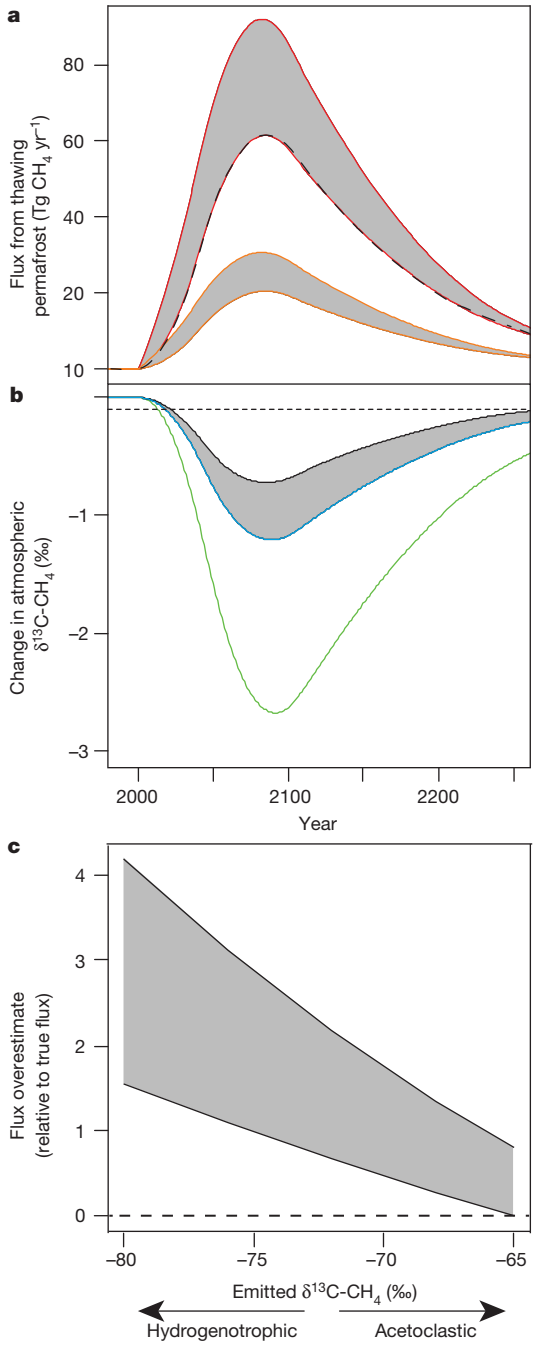

Figure 3 | Simulated effect of CH_4 from different methanogen communities in thawing permafrost on atmospheric $\delta^{13}C$-CH_4 in a box model of the atmosphere. **a**, Modelled CH_4 emissions under high (red bounding lines) and low (orange bounding lines) climate warming scenarios, and a range within each (grey tint) spanning high and low C-release scenarios[2]. **b**, Consequent decreases (simulated by the intermediate emissions scenario indicated by the red dashed line in **a**) in $\delta^{13}C$ of atmospheric CH_4 due to emissions dominated by hydrogenotrophic lineages, as in intermediate-thaw *Sphagnum* sites (green line, $\delta^{13}C = -80‰$), or more by acetoclasts, as in fully thawed *Eriophorum* sites (blue line, $\delta^{13}C = -65‰$). Atmospheric inversion models typically assume that emissions have $\delta^{13}C$ ranging from −60‰ (black line) to −65‰ (blue line). (The dotted horizontal line indicates the current detection limit for atmospheric CH_4 isotopes[28]). These imply an underestimate of the effect on atmospheric $\delta^{13}C$ for the given emissions scenario (blue or green). **c**, To match observed atmospheric isotopes, the box model would then require a corresponding overestimate of CH_4 flux attributed to permafrost thaw (vertical axis). The magnitude of the overestimate depends on the mismatch between model-assumed isotopic composition (upper line, −60‰; lower line, −65‰) and the actual isotopic composition produced by different communities, which ranges here along the horizontal axis from −80‰ (hydrogenotroph-dominated, as in the partly thawed *Sphagnum* sites) to −65‰ (acetoclastic, as in the fully thawed *Eriophorum* sites).

of isotopic patterns in the field (Fig. 2a). Several variables that typically differentiate bogs from fens, including pH and water table depth[18], were significant predictors of α_C; however, it was the relative abundance of '*M. stordalenmirensis*' that explained both the large range of α_C observed at the *Sphagnum* site ($R^2 = 0.7, P < 0.001$) and patterns across sites ($R^2 = 0.6, P < 0.001$). This suggests, contrary to the current practice of focusing on the functional diversity of communities, that an individual microbial lineage can have a disproportionate influence on ecosystem biogeochemistry.

Stepwise regression identified environmental variables (water table depth, peat C:N ratio and peat $\delta^{13}C$) that improved model predictions of α_C (to $R^2 = 0.8, P < 0.001$). Although confirming the central importance of '*M. stordalenmirensis*' in explaining variation in α_C (Extended Data Table 5), this model also supports the hypothesis that organic matter chemistry underlies shifts in CH_4 metabolism[9,25]. The dependence on the abundance of this lineage was evident despite the relative rather than the absolute nature of the community composition analysis, and the measurement of abundance rather than activity. We speculate that direct measures of gene expression or metabolic activity (metatranscriptomics and metaproteomics) will have an even stronger association than community composition data with isotopic signatures.

Further analysis showed that α_C is significantly correlated ($R^2 = 0.7$, $P = 0.004$) with the large range in CH_4:CO_2 production ratio (0.13–0.84) measured in anaerobic incubations of Stordalen peat (Fig. 2b). It is therefore likely that changes in the proportion of anaerobically mineralized C that ends up as CH_4—a key, but poorly constrained, parameter in global CH_4 models[26]—tracks the abundance of '*M. stordalenmirensis*', which acts as an index of the concerted changes in microbial community and organic matter chemistry that together control the efficiency of carbon metabolism.

Incorporating this understanding of the imprint of microbial communities could be crucial to both improved model prediction of future climate change CH_4 feedbacks and accurate attribution of the portion of global atmospheric CH_4 change that is derived from permafrost thaw. First, in simulating CH_4 cycling, Earth-system models typically prescribe as fixed the fraction of anaerobically metabolized carbon that becomes CH_4 (ref. 26). The lack of a basis for predicting this parameter across ecosystems and in response to climate change limits current modelling efforts[3]. Our finding that the CH_4:CO_2 production ratio is highly variable and predictable from isotopic indicators of methanogenic community composition (Fig. 2b) supports the need to improve the representation of microbial ecology in models[17,27]. Although simulating microbial population dynamics is beyond the scope of current global models, the identification of microbial lineages that predict key parameters, such as the CH_4:CO_2 ratio, provides insights that improve simulations of CH_4 biogeochemistry used to estimate global emissions.

Second, atmospheric inversion studies that use CH_4 mixing ratios and isotopes to infer global sources and sinks of atmospheric CH_4 assume that wetland microbial sources are dominated by acetate fermentation (−58‰ to −65‰), and, critically, that isotopic signatures from biological sources are constant over time[28,29]. In contrast, we observed isotopic compositions that varied across a gradient of permafrost thaw: hydrogenotrophic methanogenesis was estimated to produce about 50–75% of total CH_4 emission at Stordalen (Extended Data Table 6), with $\delta^{13}C$ averaging −80‰ (Fig. 1b). The hydrogenotrophic $\delta^{13}C$ observed at Stordalen and other Arctic wetlands[30] may be a ubiquitous characteristic of thawing permafrost, particularly during thaw stages that generate recalcitrant organic matter[9,25], such as that observed at Stordalen in the intermediate-thaw *Sphagnum* site.

To test whether these observed thaw-induced changes in microbial metabolism might be relevant for large-scale atmospheric methane dynamics,

we used a simple box model of atmospheric mixing (Methods, equation (3)) to quantify the effect of different methanogen communities within recently constructed scenarios of CH_4 emission from thawing permafrost[2] (Extended Data Fig. 2a, b). We found that if hydrogenotrophic lineages regulated CH_4 isotope patterns in permafrost thaw generally, as at Stordalen, then projected CH_4 emissions (Fig. 3a) would produce larger decreases in $\delta^{13}C$ of atmospheric CH_4 than expected from current inversion model assumptions that acetoclasts dominate emissions (Fig. 3b and Extended Data Fig. 2c, d). This in turn would constrain our simple box model to substantially overestimate the amount of CH_4 released from thawing permafrost and underestimate emissions from non-wetland sources, most notably fossil fuels (Fig. 3c). The greater the prevalence of hydrogenotrophic lineages in CH_4 emissions, the larger will be the overestimate of fluxes from thaw (Fig. 3c). The numerical size of the mis-estimation error here is illustrative; state-of-the-art three-dimensional inversion models have spatially resolved constraints that would probably force smaller flux mis-estimations. However, the general implication is that microbial effects are sufficiently important that accurate global accounting of the different sources of CH_4 under future climate change can be improved by understanding the microbial community dynamics underlying biological feedbacks in natural systems.

By showing that the abundance of key microbial lineages can be used to predict atmospherically relevant patterns in CH_4 isotopes and the proportion of carbon metabolized to CH_4 during permafrost thaw, this work establishes a basis for scaling changing microbial communities to ecosystem-scale and global-scale atmospheric isotope dynamics. It also highlights the central role of microbial ecology in ecosystem-scale responses to global change and the benefit of incorporating microbial dynamics into Earth-system models.

Online Content Methods, along with any additional Extended Data display items and Source Data, are available in the online version of the paper; references unique to these sections appear only in the online paper.

Received 19 March; accepted 22 August 2014.

1. Tarnocai, C. *et al.* Soil organic carbon pools in the northern circumpolar permafrost region. *Glob. Biogeochem. Cycles* **23,** GB2023 (2009).
2. Schuur, E. A. G. *et al.* Expert assessment of vulnerability of permafrost carbon to climate change. *Clim. Change* **119,** 359–374 (2013).
3. Ciais, P. *et al. Climate Change 2013: The Physical Science Basis. Contribution of Working Group I to the Fifth Assessment Report of the Intergovernmental Panel on Climate Change* (Cambridge University Press, 2013).
4. Johansson, T. *et al.* Decadal vegetation changes in a northern peatland, greenhouse gas fluxes and net radiative forcing. *Glob. Change Biol.* **12,** 2352–2369 (2006).
5. Christensen, T. R. *et al.* Thawing sub-arctic permafrost: effects on vegetation and methane emissions. *Geophys. Res. Lett.* **31,** L04501 (2004).
6. Mondav, R. *et al.* Discovery of a novel methanogen in thawing permafrost. *Nature Commun.* **5,** 3212, http://dx.doi.org/10.1038/ncomms4212 (14 February 2014).
7. Melton, J. R. *et al.* Present state of global wetland extent and wetland methane modelling: conclusions from a model inter-comparison project (WETCHIMP). *Biogeosciences* **10,** 753–788 (2013).
8. Jorgenson, M. T., Racine, C. H., Walters, J. C. & Osterkamp, T. E. Permafrost degradation and ecological changes associated with a warming climate in central Alaska. *Clim. Change* **48,** 551–579 (2001).
9. Hodgkins, S. B. *et al.* Changes in peat chemistry associated with permafrost thaw increase greenhouse gas production. *Proc. Natl Acad. Sci. USA* **111,** 5819–5824 (2014).
10. Olefeldt, D., Turetsky, M. R., Crill, P. M. & McGuire, A. D. Environmental and physical controls on northern terrestrial methane emissions across permafrost zones. *Glob. Change Biol.* **19,** 589–603 (2012).
11. Lee, H., Schuur, E. A. G., Inglett, K. S., Lavoie, M. & Chanton, J. P. The rate of permafrost carbon release under aerobic and anaerobic conditions and its potential effects on climate. *Glob. Change Biol.* **18,** 515–527 (2012).
12. Mackelprang, R. *et al.* Metagenomic analysis of a permafrost microbial community reveals a rapid response to thaw. *Nature* **480,** 368–371 (2011).
13. Riley, W. J. *et al.* Barriers to predicting changes in global terrestrial methane fluxes: analyses using CLM4Me, a methane biogeochemistry model integrated in CESM. *Biogeosciences* **8,** 1925–1953 (2011).
14. Koven, C. D. *et al.* Permafrost carbon-climate feedbacks accelerate global warming. *Proc. Natl Acad. Sci. USA* **108,** 14769–14774 (2011).
15. Turetsky, M. R., Wieder, R. K. & Vitt, D. H. Boreal peatland C fluxes under varying permafrost regimes. *Soil Biol. Biochem.* **34,** 907–912 (2002).
16. Bäckstrand, K. *et al.* Annual carbon gas budget for a subarctic peatland, northern Sweden. *Biogeosciences* **7,** 95–108 (2010).
17. Bridgham, S. D., Cadillo-Quiroz, H., Keller, J. K. & Zhuang, Q. Methane emissions from wetlands: biogeochemical, microbial, and modeling perspectives from local to global scales. *Glob. Change Biol.* **19,** 1325–1346 (2013).
18. Hornibrook, E. R. C. & Bowes, H. L. Trophic status impacts both the magnitude and stable carbon isotope composition of methane flux from peatlands. *Geophys. Res. Lett.* **34,** 2–6 (2007).
19. Chanton, J. P., Chaser, L. C., Glaser, P. & Siegel, D. in *Stable Isotopes and Biosphere–Atmosphere Interactions* (eds Flanagan, L. B., Ehleringer, J. R. & Pataki, D. E.) 85–105 (Elsevier, 2005).
20. Whiticar, M. J. Carbon and hydrogen isotope systematics of bacterial formation and oxidation of methane. *Chem. Geol.* **161,** 291–314 (1999).
21. Popp, T. J., Chanton, J. P., Whiting, G. J. & Grant, N. Methane stable isotope distribution at a *Carex* dominated fen in North Central Alberta. *Glob. Biogeochem. Cycles* **13,** 1063–1077 (1999).
22. Whiticar, M. J., Faber, E. & Schoel, M. Biogenic methane formation in marine and freshwater environments: CO_2 reduction vs. acetate fermentation—isotope evidence. *Geochim. Cosmochim. Acta* **50,** 693–709 (1986).
23. Ferry, J. G. How to make a living by exhaling methane. *Annu. Rev. Microbiol.* **64,** 453–473 (2010).
24. Liu, Y. & Whitman, W. B. Metabolic, phylogenetic, and ecological diversity of the methanogenic archaea. *Ann. NY Acad. Sci.* **1125,** 171–189 (2008).
25. Hornibrook, E. R. C., Longstaffe, F. J. & Fyfe, W. S. Spatial distribution of microbial methane production pathways in temperate zone wetland soils: stable carbon and hydrogen isotope evidence. *Geochim. Cosmochim. Acta* **61,** 745–753 (1997).
26. Wania, R. *et al.* Present state of global wetland extent and wetland methane modelling: methodology of a model inter-comparison project (WETCHIMP). *Geoscient. Model Devel.* **6,** 617–641 (2013).
27. Wieder, W. R., Bonan, G. B. & Allison, S. D. Global soil carbon projections are improved by modelling microbial processes. *Nature Clim. Change* **3,** 909–912 (2013).
28. Kai, F. M., Tyler, S. C., Randerson, J. T. & Blake, D. R. Reduced methane growth rate explained by decreased Northern Hemisphere microbial sources. *Nature* **476,** 194–197 (2011).
29. Bousquet, P. *et al.* Contribution of anthropogenic and natural sources to atmospheric methane variability. *Nature* **443,** 439–443 (2006).
30. Hines, M. E., Duddleston, K. N., Rooney-Varga, J. N., Fields, D. & Chanton, J. P. Uncoupling of acetate degradation from methane formation in Alaskan wetlands: connections to vegetation distribution. *Glob. Biogeochem. Cycles* **22,** 1–12 (2008).

Supplementary Information is available in the online version of the paper.

Acknowledgements We thank the Abisko Scientific Research Station for infrastructure and logistical support; T. Logan and N. Rakos for their assistance in the field; and S. Wofsy and S. Frolking for feedback on a draft of this paper. This work was supported by the US Department of Energy Office of Biological and Environmental Research (award DE-SC0004632), and by the University of Arizona Technology and Research Initiative Fund, through the Water, Environmental and Energy Solutions Initiative. R.M. was supported by an Australian Postgraduate Award Scholarship.

Author Contributions S.R.S., V.I.R., P.M.C., J.C. and G.W.T. designed the study. C.K.M., S.B.H., R.A.W., P.M.C., J.C. and S.R.S. designed and/or performed flux/porewater/isotope measurements and laboratory incubations. C.K.M., B.J.W., R.M., E.-H.K., S.R.S., V.I.R. and G.W.T. designed and/or performed analyses integrating bioinformatics and biogeochemistry. C.K.M., V.I.R. and S.R.S. wrote the paper in consultation with B.J.W., S.B.H., J.C., P.M.C., E.-H.K., R.M. and G.W.T.

Author Information Amplicon sequencing data are deposited in the NCBI Sequence Read Archive with accession number SRP042265. Reprints and permissions information is available at www.nature.com/reprints. The authors declare no competing financial interests. Readers are welcome to comment on the online version of the paper. Correspondence and requests for materials should be addressed to C.K.M. (carmody.mccalley@unh.edu) or S.R.S. (saleska@email.arizona.edu).

METHODS

Site description and permafrost thaw. Stordalen is a sub-arctic palsa mire located 10 km east of Abisko in the discontinuous permafrost zone of northern Sweden (68° 21′ N, 18° 49′ E, altitude 363 m above sea level). This work focuses on three distinct subhabitats, common to northern wetlands and together covering about 98% of the mire's surface: permafrost-dominated, well-drained palsas occupied by feather mosses and ericaceous and woody plants, covering 49% of the mire; intermediate permafrost sites with variable water table depth, dominated by *Sphagnum* spp., covering 37% of the mire; and full summer-thaw, wet sites with *Eriophorum angustifolium,* covering 12% of the mire. Between 1970 and 2000, as permafrost thawed and palsas collapsed, *Sphagnum* sites and *Eriophorum* sites expanded by 3% and 54%, respectively[4].

The formation of wetlands after permafrost thaw, as observed at Stordalen, is a widespread characteristic of peatlands affected by permafrost loss[8,31–33]. Thawing of ice-rich features results in peatland collapse and the formation of bogs and fens. At Stordalen, thaw is associated with a progression from ombrotrophic bogs to minerotrophic fens due to thaw-induced subsidence increasing hydrological connectivity. A similar successional shift from bogs dominated by *Sphagnum* spp. to tall graminoid fens has been observed in other northern peatlands[8,33–35]. More generally, landscape features and hydrological conditions dictate the characteristics and trajectory of wetland communities formed after permafrost thaw[36]. For example, rapid fen development is observed at the subsiding margins of permafrost plateaux[37], whereas collapse bogs and thermokarst lakes often form within large, thawing peatland complexes[32]. Large uncertainty in model predictions of the extent and characteristics of wetland formation arising from permafrost thaw is a critical limitation to current understanding of carbon–climate feedbacks[7,14]. As demonstrated in this study, improved characterization and modelling of peatland transformation during thaw will be essential for accurately predicting post-thaw microbial communities and the resultant magnitude and isotopic composition of CH_4 emissions under climate change.

Methane isotope systematics. We use standard δ notation for quantifying the isotopic compositions of CH_4 and CO_2: the ratio R of ^{13}C to ^{12}C (or D to H) in the measured sample is expressed as a relative difference (denoted $\delta^{13}C$ or δD) from the Vienna Pee Dee Belemnite (VPDB) international standard material. For example, for C:

$$\delta^{13}C = \frac{R - R_{VPDB}}{R_{VPDB}} = \frac{R}{R_{VPDB}} - 1 \quad (1)$$

$\delta^{13}C$ is often expressed in parts per thousand (‰).

Isotopic fractionation in chemical reactions (including methanogenesis or methanotrophy) or due to diffusion may be quantified as

$$\alpha = \frac{R_{source}}{R_{product}} = \frac{\delta_{source} + 1}{\delta_{product} + 1} \quad (2)$$

For diffusive fractionation, R_{source} is taken to be the isotopic ratio in the concentrations of the gradient and $R_{product}$ the ratio in the resultant net flux. Because diffusion discriminates against the heavy isotope, $R_{product} < R_{source}$, which implies, for example, that the isotopic ratio of porewater (the 'source') will be greater than that of the flux of gas diffusing out, as we see here (Fig. 1a). Methanogenesis and methanotrophy also discriminate against the heavier isotopes, so that $R_{product} < R_{source}$ (and hence $\alpha > 1$) for both C and H in methane. Note that $\alpha > 1$ for methanotrophy implies that the products of CH_4 oxidation (CO_2 and H_2O) are lighter (have lower R) in both C and H relative to the source CH_4; however, mass balance then requires the residual methane not oxidized to become heavier in both C and H relative to the starting composition of the CH_4 pool before oxidation.

The degree of C isotopic fractionation between CO_2 and CH_4 differs between the two main biochemical pathways of methanogenesis, namely acetoclastic ($CH_3COOH \rightarrow CH_4 + CO_2$) and hydrogenotrophic ($CO_2 + 4H_2 \rightarrow 2H_2O + CH_4$). Carbon isotope fractionation (α_C) is greater for hydrogenotrophic than for acetoclastic methanogenesis, but α_H (hydrogen isotope fractionation) follows the opposite pattern: α_H (hydrogenotrophic) $< \alpha_H$ (acetoclastic) (Extended Data Fig. 1; ref. 19). Hence, variations in C and H isotopic compositions of CH_4 that arise from variations in methanogenic pathway will be anti-correlated: shifts from hydrogenotrophic to acetoclastic production will cause C isotope ratios to increase but H isotope ratios to decline, moving along a negatively sloped 'production line' in H–C isotope space (Extended Data Fig. 1). Isotopic variations that arise from variations in the degree of methanotrophy, by contrast, will be positively correlated: shifts towards increasing methanotrophy will cause both C and H isotope ratios to increase along a positively sloped 'oxidation line' (Extended Data Fig. 1).

In a field study such as this, it is difficult to estimate fractionation factors directly; we therefore follow standard practice in the methane biogeochemistry literature (see, for example, refs 22, 38) and estimate the net or effective fractionation factor from *in situ* pore water data. For example, we estimate α_C, the effective fractionation factor for C in CH_4, by applying equation (2), setting $\delta_{product} = \delta^{13}C_{CH_4}$ and $\delta_{source} = \delta^{13}C_{CO2}$, where $\delta^{13}C_{CH_4}$ and $\delta^{13}C_{CH_4}$ are the observed C compositions of CH_4 and CO_2, respectively[38]. Using CO_2 isotope composition for δ_{source} follows directly for hydrogenotrophic methanogenesis (for which CO_2 is the source C substrate) and has been found to work also in practice for acetoclastic methanogenesis, because porewater CO_2 arises primarily from respiration of organic matter (a non-discriminatory reaction), and so is typically isotopically indistinguishable from organic matter[20,39].

Autochamber measurements. The autochamber system at Stordalen mire has previously been described in detail for measurements of CO_2 and total hydrocarbons[16,40]. In brief, a system of eight automatic gas-sampling chambers made of transparent Lexan was installed in the three habitat types at Stordalen mire in 2001 ($n = 3$ each in the palsa and *Sphagnum* habitats, and $n = 2$ in the *Eriophorum* habitat). Each chamber covers an area of 0.14 m^2 (38 cm × 38 cm), with a height of 25–45 cm, and is closed once every 3 h for a period of 5 min. The chambers are connected to the gas analysis system, located in an adjacent temperature controlled cabin, by 3/8-inch Dekoron tubing through which air is circulated at approximately 2.5 l min^{-1}. During the 2011 season the system was updated with a new chamber design similar to that described in ref. 41. The new chambers each cover an area of 0.2 m^2 (45 cm × 45 cm), with a height ranging from 15 to 75 cm depending on habitat vegetation. At the Palsa and *Sphagnum* site the chamber base is flush with the ground and the chamber lid (15 cm in height) lifts clear of the base between closures. At the *Eriophorum* site the chamber base is raised 50–60 cm on Lexan skirts to accommodate vegetation of large stature. In addition, each chamber is instrumented with thermocouples measuring air and surface ground temperature, and the depth of the water table is measured manually three to five times per week. The Palsa site chambers are located within the palsa site in ref. 6 and correspond to the hummock site class (I) described in ref. 4. The *Sphagnum* site chambers are located within the bog site in ref. 6 or site S in ref. 9 and correspond to the semi-wet and wet site classes (II and III) described in ref. 4. The *Eriophorum* site chambers are located within the fen site in ref. 6 or site E in ref. 9 and correspond to the tall graminoid site class (IV) described in ref. 4.

Quantum cascade laser spectrometer measurement and calibration. Methane fluxes and isotopes were measured with a quantum cascade laser spectrometer (QCLS; Aerodyne Research Inc.), deployed to Stordalen mire in June 2011. The QCLS instrument at Stordalen is a modification of the technology described in detail in ref. 42. In brief, the QCLS uses a room-temperature continuous-wave mid-infrared laser whose frequency was tuned to scan rapidly (900 kHz) across $^{12}CH_4$ and $^{13}CH_4$ absorption lines in the 7.5-μm region. The laser light enters a multipass sample cell (effective path length about 200 m) containing sample air at low pressure (about 5 kPa) and is detected by a thermoelectrically cooled detector (no cryogens are needed). Aerodyne Research's custom TDL Wintel software averages high-frequency spectra to produce independent $^{12}CH_4$ and $^{13}CH_4$ mixing ratios in the sample airstream at 1-s intervals. The ratio R of $^{13}CH_4$ to $^{12}CH_4$ can then be expressed in standard notation as $\delta^{13}C$, the part-per-thousand (‰) deviation of the measured ratio from the VPDB standard $^{13}C/^{12}C$ ratio R_{VPDB}, as in equation (1).

Instrument precision in the field at Stordalen mire was assessed by using time-series measurements of calibration tank air over 30–40 min. The precision of $\delta^{13}C$-CH_4 measurements using a 1-s integration time was 1‰. The Allan variance technique (used to characterize the minimum possible measurement error and the averaging time required to achieve it[43]), showed that the minimum measurement error on $\delta^{13}C$-CH_4 was less than 0.2‰, achieved with 60 s of averaging time. This approaches the precision of comparable measurements made with gas chromatography–isotope ratio mass spectrometry (GC–IRMS).

We connected the QCLS to the main autochamber circulation with ¼-inch Dekoron tubing and a solenoid manifold that enabled selection between the autochamber flow and an array of calibration tanks. During measurement periods, filtered (0.45 μm Teflon filter) and dried (Perma Pure PD-100T-24MSA) sample air flows at 1.4 standard litres per minute through the 2-litre QCLS sample cell volume at 5.6 kPa. A downstream solenoid controls the QCLS return flow so that air recirculates only during autochamber measurement periods; during calibration periods, exhaust air is vented to the room.

Calibrations were performed every 60 min with three calibration gases spanning the observed concentration range (1.5–10 p.p.m.). The CH_4 concentration and $\delta^{13}C$ composition of each calibration tank was determined by inter-calibration with a set of four well-characterized primary standard tanks. The primary tanks (Scott Marin, Inc.) were calibrated to the VPDB scale by means of flask samples, which were analysed by GC–IRMS at Florida State University (see porewater methods for GC–IRMS details). Each isotopologue, $^{12}CH_4$ and $^{13}CH_4$, was treated as an independent measurement and calibrated separately. For each calibration period a linear calibration curve was fitted for each isotopologue and the fit parameters were then linearly interpolated between calibration periods. The interpolated fit parameters were applied

to the measured sample isotopologue mixing ratios to give calibrated measurements of $^{12}CH_4$, $^{13}CH_4$ and total CH_4, from which $\delta^{13}C$-CH_4, was calculated.

Autochamber data processing. For each autochamber closure we calculated the flux and $\delta^{13}C$ signature of emitted CH_4. Fluxes were calculated by using a method consistent with that detailed in ref. 44 for CO_2 and total hydrocarbons, using a linear regression of changing headspace CH_4 concentration over a period of 2.5 min. Eight 2.5-min regressions were calculated, staggered by 15 s, and the most linear fit (highest r^2) was then used to calculate flux. Keeling plots[45–47] using the entire closure period were used to estimate the isotopic composition of the emitted CH_4. As demonstrated in ref. 42, negligible error in measurement of CH_4 relative to that of $\delta^{13}CH_4$ for this instrumentation meant that type I regression was sufficient for the Keeling plot analysis. When the total change in headspace CH_4 was low[45], there was high error in the Keeling intercept. We used a threshold of 3‰ uncertainty in the Keeling intercept as a cutoff for including isotopic values in the calculation of daily and annual averages, resulting in a total of 1,569 observations at the *Sphagnum* site and 1,168 at the *Eriophorum* site. No Palsa chamber closures had sufficient CH_4 flux to calculate $\delta^{13}CH_4$. Daily and whole-season average flux and isotopic composition for each habitat were calculated on the basis of individual chambers as the unit of replication ($n = 3$ for Palsa and *Sphagnum*, $n = 2$ for *Eriophorum*). Significant differences in the magnitude and isotopic composition of CH_4 emissions were determined with Student's *t*-test (isotopic composition) and analysis of variance (flux magnitude) in R[48], with seasonal averages for each autochamber as the unit of replication. Statistical significance was determined at $\alpha = 0.05$.

Porewater sampling and analysis. Porewater samples were collected on 12 July 2011, 15 August 2011 and 15 October 2011 at three locations adjacent to the *Sphagnum* and *Eriophorum* autochamber sites (Extended Data Table 1). Samples were collected by suction with a syringe through a stainless steel tube and filtered through 25-mm diameter Whatman Grade GF/D glass microfibre filters (2-μm particle retention). Porewater pH was measured in the field (Oakton Waterproof pHTestr 10; Eutech Instruments). Samples for the analysis of the concentration and $\delta^{13}C$ of CH_4 and CO_2 were injected into 30-ml evacuated vials sealed with butyl rubber septa and frozen within 8 h of collection. The samples for δD-CH_4 were injected into 120-ml evacuated vials sealed with butyl rubber septa and containing 0.5 g of KOH. For δD-H_2O, water was filtered directly into 2-ml plastic screw-cap vials so that the vials were completely filled, then frozen within 8 h of collection. All samples were shipped frozen to Florida State University for analysis.

Samples collected for analysis of CH_4 and CO_2 concentrations and $\delta^{13}C$ were thawed, acidified with 0.5 ml of 21% H_3PO_4, and brought to atmospheric pressure with helium. The sample headspace was analysed for concentrations and $\delta^{13}C$ of CH_4 and CO_2 on a continuous-flow Hewlett-Packard 5890 gas chromatograph (Agilent Technologies) at 40 °C coupled to a Finnigan MAT Delta S isotope ratio mass spectrometer via a Conflo IV interface system (Thermo Scientific). The headspace gas concentrations were converted to porewater concentrations on the basis of their known extraction efficiencies, defined as the proportion of formerly dissolved gas in the headspace. An extraction efficiency of 0.95 (based on repeated extractions) was used for CH_4, and the extraction efficiency for CO_2 relative to dissolved inorganic carbon (DIC) was determined on the basis of CO_2 extraction from dissolved bicarbonate standards[49].

Samples collected for analysis of δD-CH_4 were brought to atmospheric pressure with helium and measured on a gas chromatograph connected to a ThermoFinnegan Delta Plus continuous-flow isotope ratio mass spectrometer at the National High Magnetic Field Laboratory (Tallahassee, FL). δD of CH_4 is affected by δD of H_2O because CH_4 exchanges H atoms with water during methanogenesis[20,38,50], so measurement of δD-H_2O is necessary for the correct assignment of CH_4 production mechanisms and oxidation based on δD and $\delta^{13}C$ of CH_4. Samples collected for δD-H_2O were measured on an LGR DT-100 liquid water stable isotope analyser at Florida Agricultural and Mechanical University (Tallahassee, FL). Data analysis for these samples was performed with an MS Excel template from the IAEA Water Resources Programme (http://www.iaea.org/water).

Significant differences in α_C and δD and $\delta^{13}C$ of porewater CH_4 between the *Sphagnum* and *Eriophorum* sites were determined with Student's *t*-test (α_C, δD-CH_4, $\delta^{13}C$-CH_4) and Hotelling's *t*-test (multivariate δD and $\delta^{13}C$ of CH_4) in R[48]. Statistical significance was determined at $\alpha = 0.05$.

Peat sampling. Peat samples were collected on 12 July 2011, 16 August 2011 and 16 October 2011 at three locations adjacent to the Palsa, *Sphagnum* and *Eriophorum* autochamber sites. For the *Sphagnum* and *Eriophorum* sites, samples were collected at the same depths and locations as those used for porewater sampling (Extended Data Table 1); sample depths for the Palsa site are detailed in ref. 6. Peat cores were collected with a push corer 11 cm in diameter (Palsa and *Sphagnum* sites) or a 10 cm × 10 cm Wardenaar corer (*Eriophorum* site). Cores were subsampled by depth and were subdivided in the field for microbial and chemical analysis, avoiding the outer 1 cm of the core. Samples for microbial analysis were placed in cryotubes, saturated with about 3 volumes of LifeGuard solution (MoBio Laboratories) and stored at −80° C until processing. Samples for chemical analysis were placed in plastic bags and frozen until processing.

Peat chemical analysis. For peat %C, %N, C:N ratio and $\delta^{13}C$ measurements, 5–10 g of peat was dried at 60 °C until completely dry (3–10 days) and ground to a fine powder. Subsamples of ground peat (80–100 μg for %C and $\delta^{13}C$ analysis, and 5–6 mg for %N analysis) were wrapped in tin capsules and analysed by combustion to CO_2 and N_2 at 1,020 °C in an automated CHN elemental analyser coupled with a ThermoFinnegan Delta XP isotope ratio mass spectrometer at the National High Magnetic Field Laboratory. Samples were run in non-dilution mode for carbon analysis and dilution mode (×10) for nitrogen analysis. C:N was calculated as (%C)/(%N) (by weight) for corresponding pairs of subsamples.

Small-subunit ribosomal RNA gene amplicon analysis. Sampling and extraction was performed as described previously[6]. Several additional samples were analysed for this paper; multiplex identifiers for those runs not reported in ref. 6 are provided in Extended Data Table 7. Small-subunit rRNA gene sequences were processed with APP 3.0.3 (https://github.com/Ecogenomics/APP). Homopolymer errors were corrected with Acacia[51] and the resulting reads were processed by using the CD-HIT-OTU 0.0.2 pipeline with minor adjustments[52]. All reads were trimmed to 250 base pairs, and reads of less than 250 base pairs were discarded. Sequences were clustered at 97% identity and each cluster was assigned a taxonomy using BLASTN 2.2.22 (ref. 53) through the QIIME script assign_taxonomy.py[54] against the GreenGenes October 2012 database clustered at 99% identity (Supplementary Table 1). The taxonomy of each methanogenic cluster was confirmed by using parsimony insertion in ARB[55]. Amplicon sequence clusters were identified as potential hydrogenotrophic or acetoclastic methanogens based on taxonomic relationship to known methanogenic lineages (Extended Data Table 2)[23,24,56]. Within the order *Methanosarcinales*, lineages most closely related to *Methanosaeta* were classified as obligate acetoclasts, whereas those most closely related to *Methanosarcina* were considered facultative acetoclasts, having the potential for both acetoclastic or hydrogenotrophic production[23].

Regression analysis. A stepwise regression approach with Akaike's information criterion (AIC) as the model selection criterion was used to identify a subset of microbial and environmental predictor variables that best explained CH_4 metabolism patterns quantified as porewater α_C (Extended Data Table 5). Model selection was performed with the stepAIC package in R, and the relative importance of the predictor variables in the selected model was then calculated with the relaimpo R package[48]. Variables included in the model selection process included the relative abundances of the six most abundant methanogen operational taxonomic units (comprising more than 93% of the total methanogen sequences; see Extended Data Table 2) plus soil temperature, water table depth, pH, porewater CH_4 and DIC concentration, and peat C:N, %C, %N and $\delta^{13}C$ (Extended Data Table 1). Strong correlation between pH and both water-table depth and peat $\delta^{13}C$ as well as peat %N and both %C and C:N meant that pH and %N were excluded from the regression analysis. Removal of non-significant predictor variables (DIC and relative abundance of an unidentified *Methanobacterium* spp. (otu-3636; Extended Data Table 2)) had a minimal effect on the model AIC value (less than 1); this simplified version was therefore selected as the optimal model (model 2 in Extended Data Table 5). Stepwise regression was also performed with $\delta^{13}C$-CH_4 as the dependent variable. This analysis resulted in a similar model outcome, but with a lower R^2 (model 1 in Extended Data Table 8). Stepwise regression analysis with environmental predictor variables and the relative abundance of the influential methanogen '*M. stordalenmirensis*' (otu-10747) as the dependent variable showed that patterns in this methanogen's abundance were influenced by environmental conditions, particularly water table depth and peat chemistry (model 2 in Extended Data Table 8). However, these environmental variables alone cannot fully replace microbial data when modelling α_C. Stepwise regression analysis using only environmental variables to predict α_C yielded a model with a lower AIC and R^2 (model 3 in Extended Data Table 8). It is the combination of methanogen and environmental variables that yields a model that explains the most variability in α_C (Extended Data Table 5).

Box model of atmospheric methane. The model used here was a one-box model simplified from the two-box model of ref. 57 (and also used in the methane inversion study[28]):

$$\frac{dM}{dt} = F_{CH_4} - \lambda M \tag{3}$$

$$\frac{d(RM)}{dt} = R_{CH_4} F_{CH_4} - \alpha_{OH} \lambda (RM)$$

where M is the mixing ratio (in p.p.b.v.) of CH_4 in the atmosphere, F_{CH_4} is the source flux of CH_4 to the atmosphere, λ is the atmospheric removal rate ($1/9\ yr^{-1}$, assumed for this illustration to be fixed), the R terms are the ratio of $^{13}CH_4$ to $^{12}CH_4$, as defined for equation (1), and α_{OH} is the isotopic fractionation (0.994, or

about −6‰) for the atmospheric oxidation of CH_4 by OH (ref. 28). Baseline flux to the atmosphere (F_{CH_4}) was set to 559 Tg CH_4, the 1980 value[28]. The isotopic composition of CH_4 inputs to the atmosphere (R_{CH_4}) was set to the equivalent of −53‰ to allow steady-state modern atmospheric CH_4 to have the observed value of about −47‰.

We implemented this model numerically in the R software package[48], simulating the effect on the atmosphere of CH_4 emission due to permafrost thaw and partial decomposition of the 1,700 Pg C stock of permafrost C expected over the next 300 years, as summarized in refs 1, 2. High and low permafrost carbon release scenarios for both the high climate change scenario (Intergovernmental Panel on Climate Change (IPCC) scenario RCP8.5, leading to the release of 120–195 Pg C) and the low climate change scenario (IPCC scenario RCP2.6, approximated as one-third of the C release of the high scenario) (Extended Data Fig. 2a) generated CH_4 emissions (Fig. 3a) (based on 2.3% of released permafrost carbon emerging as CH_4 (ref. 2)) and corresponding impacts on the atmospheric concentrations of CH_4 (Extended Data Fig. 2b). We simulated the impacts of these emissions on the isotopic composition of atmospheric CH_4 by assuming that the $\delta^{13}C$ of CH_4 emitted was in the range of what we report here for Stordalen mire, from very light (−80‰, like that measured at the *Sphagnum* site) to only moderately light (−65‰, like that measured at the *Eriophorum* site), giving a range of isotopic perturbations to atmospheric CH_4 under high climate change (Extended Data Fig. 2c) and under low climate change (Extended Data Fig. 2d). In all scenarios, the induced change in atmospheric $\delta^{13}C$ is significantly larger than the atmospheric detection limit of 0.1‰ (reported in ref. 28 and shown as a dotted horizontal line in Extended Data Fig. 2c, d).

For the analysis shown in Fig. 3 we focused on a mid-range value of permafrost C release (high climate change scenario with low C release, 120 Pg total C by 2100), corresponding to emissions of 2.8 Pg C as CH_4 by 2100 (the dashed black and red line in Fig. 3a). (By comparison, the IPCC estimates that up to 5 Pg C may be released as CH_4 by 2100 (ref. 3).) We explored the misattribution of C release that would occur, by (mistakenly) assuming that the isotopic composition of emitted CH_4 was in the range of assumptions used in previous atmospheric inversions, from −60‰ to −65‰ (ref. 28), instead of the range measured at Stordalen mire (−65‰ to −80‰). We estimated the magnitude of misattribution (or error flux; Fig. 3c) by simulating the amount of additional carbon that would need to be released (at nominally assumed isotopic composition values of −60 or −65) to have the same effect on atmospheric composition as the carbon released under scenarios with isotopic compositions like those observed in the field.

31. Payette, S. Accelerated thawing of subarctic peatland permafrost over the last 50 years. *Geophys. Res. Lett.* **31,** 1–4 (2004).
32. O'Donnell, J. a. *et al.* The effects of permafrost thaw on soil hydrologic, thermal, and carbon dynamics in an Alaskan peatland. *Ecosystems* **15,** 213–229 (2012).
33. Vitt, D. H., Halsey, L. A. & Zoltai, S. C. The changing landscape of Canada's western boreal forest: the current dynamics of permafrost. *Can. J. For. Res.* **30,** 283–287 (2000).
34. Quinton, W. L., Hayashi, M. & Chasmer, L. E. Permafrost-thaw-induced land-cover change in the Canadian subarctic: implications for water resources. *Hydrol. Processes* **25,** 152–158 (2011).
35. Zoltai, S. C. Cyclic development of permafrost in the peatlands of Northwestern Alberta, Canada. *Arct. Alp. Res.* **25,** 240–246 (1993).
36. Camill, P. & Clark, J. S. Climate change disequilibrium of boreal permafrost peatlands caused by local processes. *Am. Nat.* **151,** 207–222 (1998).
37. Dyke, L. D. & Sladen, W. E. Permafrost and peatland evolution in the Northern Hudson Bay Lowland, Manitoba. *Arctic* **63,** 429–441 (2010).
38. Whiticar, M. J. & Faber, E. Methane oxidation in sediment and water column environments—isotopic evidence. *Org. Geochem.* **10,** 759–768 (1986).
39. Conrad, R. Quantification of methanogenic pathways using stable carbon isotopic signatures: a review and a proposal. *Org. Geochem.* **36,** 739–752 (2005).
40. Bäckstrand, K., Crill, P. M., Mastepanov, M., Christensen, T. R. & Bastviken, D. Non-methane volatile organic compound flux from a subarctic mire in Northern Sweden. *Tellus B Chem. Phys. Meterol.* **60,** 226–237 (2008).
41. Bubier, J. L., Crill, P. M., Mosedale, A., Frolking, S. & Linder, E. Peatland responses to varying interannual moisture conditions as measured by automatic CO_2 chambers. *Glob. Biogeochem. Cycles* **17,** 1066, http://dx.doi.org/10.1029/2002GB001946 (2003).
42. Santoni, G. W. *et al.* Mass fluxes and isofluxes of methane (CH_4) at a New Hampshire fen measured by a continuous wave quantum cascade laser spectrometer. *J. Geophys. Res.* **117,** D10301 (2012).
43. Werle, P., Mücke, R. & Slemr, F. The limits of signal averaging in atmospheric trace-gas monitoring by tunable diode-laser absorption spectroscopy (TDLAS). *Appl. Phys. B* **139,** 131–139 (1993).
44. Bäckstrand, K., Crill, P. M., Mastepanov, M., Christensen, T. R. & Bastviken, D. Total hydrocarbon flux dynamics at a subarctic mire in northern Sweden. *J. Geophys. Res.* **113,** G03026, http://dx.doi.org/10.1029/2008JG000703 (2008).
45. Pataki, D. E. The application and interpretation of Keeling plots in terrestrial carbon cycle research. *Glob. Biogeochem. Cycles* **17,** 1022, http://dx.doi.org/10.1029/2001GB001850 (2003).
46. Keeling, C. D. The concentration and isotopic abundances of atmospheric carbon dioxide in rural areas. *Geochim. Cosmochim. Acta* **13,** 322–334 (1958).
47. Keeling, C. D. The concentration and isotopic abundances of carbon dioxide in rural and marine air. *Geochim. Cosmochim. Acta* **24,** 277–298 (1960).
48. R Development Core Team. *A Language and Environment for Statistical Computing* (R Foundation for Statistical Computing, 2012).
49. Corbett, J. E. *et al.* Partitioning pathways of CO_2 production in peatlands with stable carbon isotopes. *Biogeochemistry* **114,** 327–340 (2013).
50. Chanton, J. P., Fields, D. & Hines, M. E. Controls on the hydrogen isotopic composition of biogenic methane from high-latitude terrestrial wetlands. *J. Geophys. Res.* **111,** 1–9 (2006).
51. Bragg, L., Stone, G., Imelfort, M., Hugenholtz, P. & Tyson, G. W. Fast, accurate error-correction of amplicon pyrosequences. *Nature Methods* **9,** 425–426 (2012).
52. Li, W. & Godzik, A. Cd-hit: a fast program for clustering and comparing large sets of proteins or nucleotide sequences. *Bioinformatics* **22,** 1658–1659 (2006).
53. Altschul, H. J. *et al.* Gapped BLAST and PSI-BLAST: a new generation of protein database search programs. *Nucleic Acids Res.* **25,** 3389–3402 (1997).
54. Caporaso, J. G. *et al.* QIIME allows analysis of high-throughput community sequencing data. *Nature Methods* **7,** 335–336 (2010).
55. Ludwig, W. *et al.* ARB: a software environment for sequence data. *Nucleic Acids Res.* **32,** 1363–1371 (2004).
56. Conrad, R. The global methane cycle: recent advances in understanding the microbial processes involved. *Environ. Microbiol. Rep.* **1,** 285–292 (2009).
57. Tans, P. P. A note on isotopic ratios and the global atmospheric methane budget. *Glob. Biogeochem. Cycles* **11,** 77–81 (1997).

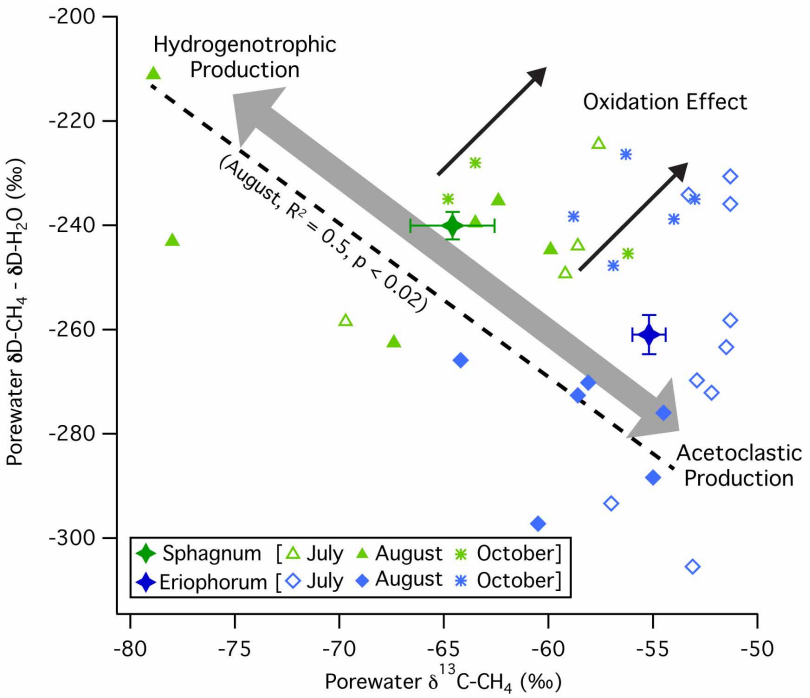

Extended Data Figure 1 | Expected and observed relationships between the δD and δ^{13}C content of porewater CH_4. The thick grey arrow shows the expected pattern in H and C isotopes of CH_4 when variations are caused by shifts between acetoclastic (lower right) and hydrogenotrophic (upper left) production. The thin black arrows pointing to the upper right indicate the expected pattern in H and C isotopes of CH_4 when variations are caused by changes in CH_4 oxidation[19]. The points are observed isotopic compositions of samples collected between July and October 2011 at the partly thawed *Sphagnum* and fully thawed *Eriophorum* sites; site averages are shown with error bars (error bars represent s.e.m.; $n = 13$ (*Sphagnum*) and 20 (*Eriophorum*)). Although the scatter allows for some variation in both production and oxidation, the average *Eriophorum* porewater CH_4 had significantly more ^{13}C and less D relative to *Sphagnum* porewater (Hotelling's T^2 test, $P = 0.0001$, $n = 33$), indicating that the overall inter-site isotopic differences were due mostly to differences in the CH_4 production pathway rather than to differences in CH_4 oxidation. Additionally, in August there was a significant negative relationship between δ^{13}C-CH_4 and δD-CH_4 of porewater samples collected across sites (dashed line, linear regression, $R^2 = 0.5$, $P < 0.02$, $n = 12$). Note that on the vertical axis δD-H_2O has been subtracted from δD-CH_4 to correct for the effect of δD exchange between H_2O and CH_4 (refs 20, 38, 50).

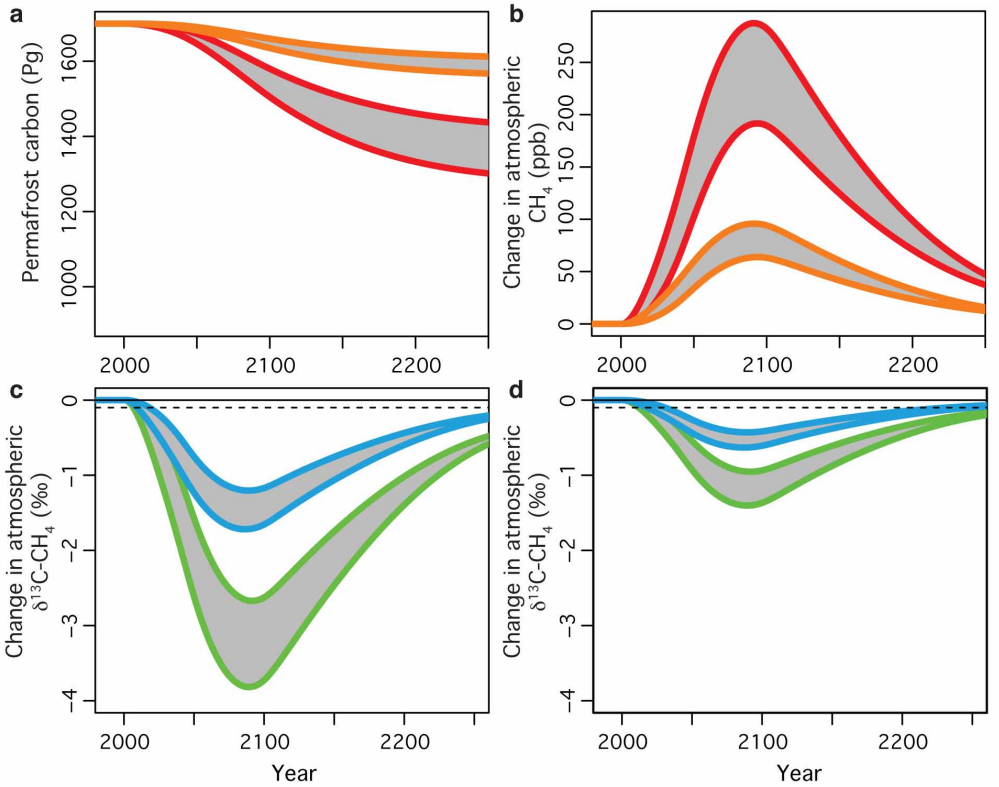

Extended Data Figure 2 | Simulations, using high and low temperature and C release scenarios, of the effect of CH_4 release from thawing permafrost on atmospheric $\delta^{13}C$-CH_4. **a**, Scenarios of permafrost C release due to thaw (red bounding lines, high temperature; orange bounding lines, low temperature; the range in each case is defined by high and low C release scenarios). **b**, Impact on atmospheric methane mixing ratios (assuming that 2.3% of released C is emitted as methane). **c**, Impact of the high climate change scenario on atmospheric methane isotopes, assuming *Eriophorum*-like emissions (blue bounding lines, $\delta^{13}C \approx -65‰$), or assuming *Sphagnum*-like emissions (green bounding lines, $\delta^{13}C \approx -80‰$). **d**, As in **c**, except for the low climate change scenario. In **c** and **d**, dotted horizontal lines indicate the detection limit for CH_4 isotopes[28].

Extended Data Table 1 | Summary of porewater chemistry, average (s.e.m.), *n* = 3

Sample	Depth (cm)	pH	mM CO_2	mM CH_4	$\delta^{13}CO_2$ ‰	$\delta^{13}CH_4$ ‰	α_C
			July, 2011				
Sphagnum - M	13	4.1 (0.06)	3.02 (0.78)	0.09 (0.04)	-15.7 (1.6)	-62.2 (3.8)	1.050 (0.005)
Sphagnum - D	19	4.2 (0.09)	3.50 (0.57)	0.15 (0.05)	-14.1 (0.6)	-62.2 (4.5)	1.051 (0.005)
Eriophorum - S	3	5.8 (0.09)	2.29 (0.92)	0.18 (0.12)	-14.1 (1.1)	-52.1 (0.5)	1.040 (0.001)
Eriophorum -M	7	5.6 (0.06)	3.06 (0.77)	0.28 (0.07)	-12.9 (1.0)	-52.6 (0.6)	1.042 (0.001)
Eriophorum - D	24	5.6 (0.03)	3.56 (0.80)	0.36 (0.07)	-11.6 (1.7)	-53.3 (1.9)	1.044 (0.004)
			August, 2011				
Sphagnum - M	21	4.2 (0.10)	4.89 (0.37)	0.23 (0.04)	-12.0 (1.5)	-66.7 (5.7)	1.059 (0.008)
Sphagnum - D	26	4.1 (0.13)	4.80 (0.48)	0.23 (0.04)	-10.7 (1.6)	-69.9 (4.6)	1.064 (0.007)
Eriophorum - S	3	5.7 (0.19)	1.62 (0.28)	0.06 (0.04)	-13.5 (0.5)	-60.0 (2.6)	1.049 (0.003)
Eriophorum -M	7	5.7 (0.10)	1.93 (0.25)	0.10 (0.02)	-13.9 (0.4)	-56.6 (2.1)	1.045 (0.002)
Eriophorum - D	26	5.6 (0.15)	3.58 (0.62)	0.31 (0.11)	-11.1 (2.4)	-55.9 (1.1)	1.047 (0.001)
			October, 2011				
Sphagnum - M	10	4.3 (0.06)	1.24 (0.42)	0.03 (0.02)	-16.4 (1.6)	-59.2 (6.5)	1.046 (0.006)
Sphagnum - D	15	4.5 (0.10)	3.21 (0.90)	0.10 (0.04)	-13.8 (2.4)	-61.5 (2.7)	1.051 (0.0004)
Eriophorum - S	3	5.9 (0.15)	2.15 (1.43)	0.19 (0.13)	-14.1 (1.0)	-56.4 (2.4)	1.045 (0.001)
Eriophorum -M	7	5.9 (0.15)	2.71 (1.25)	0.29 (0.14)	-13.7 (1.6)	-57.8 (3.1)	1.047 (0.002)
Eriophorum - D	26	5.7 (0.12)	3.84 (1.64)	0.53 (0.27)	-11.3 (3.1)	-58.1 (2.2)	1.050 (0.001)

Extended Data Table 2 | Relative abundance, taxonomic classification and predicted methanogenic pathway of the dominant methanogen operational taxonomic units (OTUs)

Sample	Candidatus *Methanoflorens* (otu-10747) Hydrogenotrophic	*Methanobacterium* (otu-3636) Hydrogenotrophic	Candidatus *Methanoregula* (otu-20819) Hydrogenotrophic	*Methanosarcina* (otu-7308) Acetoclastic (facultative)	*Methanosaeta* (otu-10220) Acetoclastic (obligate)	*Methanosaeta* (otu-15150) Acetoclastic (obligate)
July, 2011						
Palsa – S	0.0	0.0	0.0	0.0	0.0	0.0
Palsa – M	0.0	0.0	0.0	0.0	0.0	0.0
Palsa – D	0.0	0.4	0.0	0.0	0.0	0.0
Sphagnum – S	0.3	0.4	0.0	0.1	0.0	0.0
Sphagnum – M	4.0	12.9	0.0	3.4	0.0	0.0
Sphagnum – D	16.4	5.8	0.0	3.3	0.0	0.0
Eriophorum – S	1.0	2.7	5.8	0.7	4.5	1.8
Eriophorum – M	5.3	3.7	4.0	2.2	5.0	2.7
Eriophorum – D	8.3	1.6	1.9	0.6	4.2	1.2
August, 2011						
Palsa – S	0.0	0.0	0.0	0.0	0.0	0.0
Palsa – M	0.0	0.0	0.0	0.0	0.0	0.0
Palsa – D	0.0	0.0	0.0	0.0	0.0	0.0
Sphagnum – S	0.1	0.4	0.0	0.2	0.0	0.0
Sphagnum – M	11.6	4.0	0.0	1.9	0.0	0.0
Sphagnum – D	32.1	3.1	0.0	1.4	0.0	0.0
Eriophorum – S	0.6	2.1	3.6	0.4	3.3	1.0
Eriophorum – M	6.3	6.1	5.1	2.6	9.0	3.9
Eriophorum – D	6.5	0.3	3.4	1.2	1.7	0.6
October, 2011						
Palsa – S	0.0	0.0	0.0	0.0	0.0	0.0
Palsa – M	0.1	1.1	0.0	0.1	0.0	0.0
Palsa – D	0.1	0.7	0.0	0.0	0.0	0.0
Sphagnum – S	0.0	0.1	0.0	0.0	0.0	0.0
Sphagnum – M	0.0	3.4	0.0	1.1	0.0	0.0
Sphagnum – D	0.6	8.4	0.0	1.2	0.0	0.0
Eriophorum – S	2.5	1.7	1.7	0.6	1.4	0.6
Eriophorum – M	2.1	1.9	1.0	0.8	2.5	2.2
Eriophorum – D	6.0	1.1	3.7	0.1	5.1	5.8

Extended Data Table 3 | Relative abundance of methanogen functional groups within the Archaea

Site	Hydrogenotrophic	Acetoclastic (facultative)	Acetoclastic (obligate)	Other Archaea
July, 2011				
Palsa	35.9	2.9	0.0	61.2
Sphagnum (aerobic)*	83.1	15.5	0.0	1.4
Sphagnum (anaerobic)†	82.1	14.2	0.0	3.8
Eriophorum	39.5	4.2	21.4	34.9
August, 2011				
Palsa	0.0	8.7	0.0	91.3
Sphagnum (aerobic)*	68.2	30.7	0.0	1.1
Sphagnum (anaerobic)†	91.2	6.1	0.0	2.8
Eriophorum	39.5	5.1	21.9	33.5
October, 2011				
Palsa	56.5	2.6	0.4	40.5
Sphagnum (aerobic)*	65.7	24.0	0.7	9.6
Sphagnum (anaerobic)†	15.6	2.8	2.6	79.0
Eriophorum	35.8	2.4	27.6	34.2

* Above the water table.
† Below the water table.

Extended Data Table 4 | Results of linear regression analysis for predicting α_C from the relative abundances of methanogenic pathways, dominant methanogenic lineages and environmental variables ($n = 41$)

Variable	R^2	F-statistic	p-value
'*M. stordalenmirensis*'	0.58	54.09	<0.001
otu-3636*	0.00	0.01	0.926
otu-10220*	0.12	5.36	0.026
otu-20819 *	0.15	6.82	0.013
otu-15150 *	0.06	2.27	0.140
otu-7308 *	0.01	0.32	0.576
Hydrogenotrophic	0.44	30.63	<0.001
Acetoclastic (obligate)	0.12	5.23	0.028
Water table depth	0.44	31.1	<0.001
pH	0.19	8.97	0.005
Porewater CH_4 (mM)	0.00	0.07	0.796
Porewater DIC (mM)	0.25	13.33	0.001
Peat C:N	0.00	0.17	0.682
Peat %C	0.02	0.75	0.393
Peat %N	0.00	0.14	0.709
Peat $\delta^{13}C$	0.13	5.99	0.019

* See Extended Data Table 2 for taxonomic details.

Extended Data Table 5 | Results of stepwise multiple regression analysis for predicting α_C from relative abundances of methanogenic lineages and environmental variables

Variable	Coefficient	Std Error	t value	p value	Cumulative AIC
Model 1 - stepwise regression, direction = both (R^2 = 0.81, F = 23.71 on 6 and 34 df, p <0.001)					
Water table depth	-0.0004	0.0001	-5.398	<0.001	-422.33
'*M. stordalenmirensis*'	0.0271	0.0084	3.221	0.002	-436.79
C:N	-0.0002	0.0001	-2.872	0.007	-438.80
Peat $\delta^{13}C$	0.0014	0.0006	2.516	0.017	-440.71
DIC (mM)	0.0007	0.0005	1.396	0.171	-445.42
otu-3636*	-0.0271	0.0161	-1.345	0.188	-445.58
Intercept	1.089	0.0167	65.193	<0.001	-445.71
Model 2 – significant predictor variables from model 1 (R^2 = 0.79, F = 33.71 on 4 and 36 df, p <0.001)					
Water table depth	-0.0004	0.0001	-5.202	<0.001	-425.11
'*M. stordalenmirensis*'	0.0351	0.0072	4.867	<0.001	-427.36
C:N	-0.0002	0.0001	-2.613	0.013	-440.97
Peat $\delta^{13}C$	0.0014	0.0006	2.470	0.018	-441.67
Intercept	1.089	0.0164	66.583	<0.001	-446.09

* See Extended Data Table 2 for taxonomic details.

Extended Data Table 6 | Estimate of the relative contribution of hydrogenotrophic production to annual CH_4 emission at Stordalen mire

Habitat	Area (ha)*	Annual Flux (g CH_4 m^{-2}) †	Annual Emission (kg CH_4) *,†	Estimated Emission from Hydrogenotrophy (kg CH_4 yr^{-1}) ‡
Sphagnum	6.2	6.2	288.3	247.9§ - 282.5‖
Eriophorum	2.0	36.0	540.6	172.8¶– 335.2#
Total			828.9	420.7(51%) – 617.7 (75%)

* Based on ref. 4; the *Sphagnum* site in this study is representative of the semi-wet and wet vegetation classes.
† Annual total hydrocarbon emissions from ref. 16 corrected for non-methane volatile organic compound (NMVOC) flux using the reported proportions (25% NMVOC for the *Eriophorum* site; 15% for the *Sphagnum* site). The magnitude of growing season CH_4 emissions measured in this study is comparable to the growing season CH_4 flux used in the estimate of annual flux in ref. 16.
‡ Two approaches: isotopic, using mixing of acetoclastic (−60‰) and hydrogenotrophic (−80‰) sources to yield mean emitted δ^{13}C-CH_4, and molecular, using the proportion of the methanogen community identified as hydrogenotrophic.
§ Molecular approach: on average 86% of methanogen community in the anoxic CH_4-producing peat was identified as hydrogenotrophic; all of the acetoclasts were facultative so this is probably an underestimate of potential hydrogenotrophic production.
‖ Isotopic approach: $-79.6‰ = -80‰ \times \mathbf{0.98} + -60‰ \times 0.02$ (the bold number indicates the proportion of CH_4 produced by hydrogenotrophy that would produce the measured δ^{13}C-CH_4).
¶ Isotopic approach: $-66.3‰ = -80‰ \times \mathbf{0.32} + -60‰ \times 0.68$ (the bold number indicates the proportion of CH_4 produced by hydrogenotrophy that would produce the measured δ^{13}C-CH_4).
#Molecular approach: on average 62% of the methanogen community was identified as hydrogenotrophic.

Extended Data Table 7 | Small-subunit rRNA gene amplicon multiplex identifiers (MIDs) used for each sample

Sample name	Run #	Multiplex identifier (MID)
20110712_E_3_M	6	CGAGC
20110712_S_1_M	6	CGCAT
20110712_S_3_M	6	CGTAC
20110712_P_1_S	6	CGTGT
20110712_P_2_S	6	CTAGT
20110712_P_3_S	6	CTGAC
20110816_S_2_S	6	TACGC
20110816_S_1_D	6	TATGT
20110816_P_1_M	6	TCAGT
20111016_P_1_S	6	TCGAT

* Sample names are composed of the date of sampling, followed by P, S or E for Palsa, *Sphagnum* or *Eriophorum* sites, respectively; the number indicates the core within the site, and S, M or D indicates surface, middle or deep sampling within the core, respectively.
† Samples were multiplexed in six separate runs, each time with samples not related to this study. The multiplex identifiers of the first five runs are given in ref. 6.

Extended Data Table 8 | Results of stepwise multiple regression analysis for predicting $\delta^{13}C\text{-}CH_4$ from relative abundances of methanogenic lineages and environmental variables (model 1), the relative abundance of '*M. stordalenmirensis*' from environmental variables (model 2), and α_C from environmental variables (model 3)

Variable	Coefficient	Std Error	t value	p value	Cumulative AIC
Model 1 - stepwise regression, dependent variable = $\delta^{13}C\text{-}CH_4$, direction = both (R^2 = 0.75, F = 21.25 on 5 and 35 df, p <0.001)					
Water table depth	0.299	0.07	4.512	<0.001	130.95
'*M. stordalenmirensis*'	-23.25	6.79	-3.426	0.002	124.01
Peat $\delta^{13}C$	-1.51	0.54	-2.779	0.009	120.33
CH_4 (mM)	10.60	4.12	2.576	0.014	119.28
C:N	0.12	0.05	2.149	0.039	117.24
Intercept	-102.14	15.23	-6.705	<0.001	114.16
Model 2 - stepwise regression, dependent variable = '*M stordalenmirensis*', direction = both (R^2 = 0.53, F = 7.77 on 5 and 35 df, p <0.001)					
Water table depth	-0.0053	0.0015	-3.634	<0.001	-188.03
C:N	-0.0035	0.0010	-3.495	0.001	-188.88
DIC (mM)	0.0214	0.0106	2.025	0.050	-196.61
% C	0.0033	0.0018	1.799	0.081	-197.53
Soil temperature	0.0059	0.0040	1.483	0.147	-198.66
Intercept	-0.0558	0.0805	-0.692	0.493	-199.15
Model 3 - stepwise regression, dependent variable = αC, direction = both (R^2 = 0.71, F = 21.71 on 4 and 36 df, p <0.001)					
Water table depth	-0.0005	0.0001	-6.465	<0.001	-402.97
C:N	-0.0003	0.0001	-4.514	<0.001	-416.18
DIC (mM)	0.0015	0.0006	2.629	0.013	-427.36
Peat $\delta^{13}C$	0.0017	0.0007	2.574	0.014	-427.63
Intercept	1.0990	0.0192	57.396	<0.001	-432.56